# Weierstraß-Institut
## für Angewandte Analysis und Stochastik
### Leibniz-Institut im Forschungsverbund Berlin e. V.

Preprint ISSN 0946 – 8633


# Gradient flow perspective of thin-film bilayer flows


Robert Huth[1], Sebastian Jachalski[1], Georgy Kitavtsev[2], Dirk Peschka[1]



submitted: July 8, 2013



[1] Weierstrass Institute
Mohrenstr. 39
10117 Berlin
Germany
E-Mail: Robert.Huth@wias-berlin.de
Sebastian.Jachalski@wias-berlin.de
Dirk.Peschka@wias-berlin.de

[2] Max Planck Institute for Mathematics in the Sciences
Inselstraße 22
04103 Leipzig
Germany
E-Mail: Georgy.Kitavtsev@mis.mpg.de



No. 1814
Berlin 2013

2010 *Mathematics Subject Classification.* 76A20, 35R37, 37D35, 35K65.

*Key words and phrases.* thin-film, gradient flow, moving boundary problem, bilayer.

This work was supported by DFG SPP 1506 and DFG Research Center MATHEON in Berlin.

Edited by
Weierstraß-Institut für Angewandte Analysis und Stochastik (WIAS)
Leibniz-Institut im Forschungsverbund Berlin e. V.
Mohrenstraße 39
10117 Berlin
Germany

Fax: +49 30 20372-303
E-Mail: preprint@wias-berlin.de
World Wide Web: http://www.wias-berlin.de/

**Abstract**

We study gradient flow formulations of thin-film bilayer flows with triple-junctions between liquid/liquid/air. First we highlight the gradient structure in the Stokes free-boundary flow and identify its solutions with the well-known PDE with boundary conditions. Next we propose a similar gradient formulation for the corresponding thin-film model and formally identify solutions with those of the corresponding free-boundary problem. A robust numerical algorithm for the thin-film gradient flow structure is then provided. Using this algorithm we compare the sharp triple-junction model with precursor models. For their stationary solutions a rigorous connection is established using $\Gamma$-convergence. For time-dependent solutions the comparison of numerical solutions shows a good agreement for small and moderate times. Finally we study spreading in the zero-contact angle case, where we compare numerical solutions with asymptotically exact source-type solutions.

# 1 Introduction to liquid-liquid thin film flows

Dewetting of thin films from a solid substrate is an intensively studied subject, both from theoretical and from experimental point of view, e.g. [1] and references therein. There is known to be an intriguing interplay between the flow and the boundary condition on the substrate. For a no-slip boundary condition at the solid interface a logarithmic singularity in the dissipation prevents the triple-junction from moving and no dewetting takes place [2, 3]. Due to the different nature of liquid substrates no such effects have been observed or are expected for liquid substrates. There is the fitting citation from the *Capillarity and wetting phenomena* book by P.G. de Gennes et al. [4] (pg. 169) explaining why liquid substrates might be just perfect to study moving contact lines:

> *"Liquid substrate, smooth and homogeneous, are the epitome of perfection. However, they deform and flow. The challenge is to take into account the flows induced by the motion of the ridge."*

Besides the classical works on liquid/liquid spreading and dewetting by Joanny [5] and Brochard-Wyart et al. [6], there are a number of works dealing with liquid substrates from a PDE perspective by using thin-film equations: Kriegsmann & Miksis [7] investigate the quasi-stationary motion of 2D-droplets on inclined substrates with gravity and sharp triple-junctions (point). Pototsky et al. wrote a series of papers, e.g. [8], where they investigate different possible stationary solutions of two-layer systems. Following the classical theory they compute multiple Hamaker constants which contribute to the van-der-Waals type precursor energy depending on the thickness of the different layers. In [9] Craster & Matar studied the approach of droplets toward equilibrium

and equilibrium shapes of droplets. They also used a precursor layer to account for the motion of the triple-junction. In a later paper Karapetsas et al. [10] study the motion of droplets with surfactants on a liquid substrate with sharp triple-junctions. Thin-film approximations for bilayer flows were initially derived by Danov and co-workers [11] and with sharp triple-junctions by Kriegsmann [12]. Existence of weak solutions was established in [13, 14].

The goal of this paper is to look at bilayer flows where triple-junctions are treated explicitly using a formal gradient flow model. Such an approach is advantageous because boundary conditions can be enforced in a rather natural way in any number of spatial dimensions. Furthermore, we can distinguish boundary conditions which are already in the solution manifold, e.g. conservation of mass, and those derived from the gradient of the driving energy, e.g. contact angles. We also connect this approach to the more popular model with precursor.

In the remainder of this section we state thin-film models for two-layer flows as they are known in the literature. In section 2 we first state a gradient formulation of the Stokes equation to motivate that such a formulation exists and how the solution manifold should be interpreted. Next we make a thin-film approximation of the driving energy. Furthermore we propose a metric on the solution manifold and identify the gradient and compare with the model of [7]. Then in section 3 we show that this formulation is well-suited for the construction of a robust numerical algorithm. We give a detailed explanation of the spatial and temporal discretization. A slightly non-standard trick is that we first compute time-derivatives in the momentary configuration and later separate them into a convective derivative and a transport of the domain. Finally, in section 4 we compare this approach to precursor models and asymptotic source-type solutions. We make rigorous statements about convergence of stationary solutions of the precursor model as the precursor thickness tends to zero. Then we use the constructed numerical algorithm to compare dynamical solutions of the gradient model with explicit triple-junction with the precursor model. For large times and zero contactangle we derive source-type solutions and compare them with our numerical simulations.

## 1.1 Thin-film equations for bilayer flows

In this section we present lubrication models for liquid films on a liquid substrate. One major difference in the following models is the treatment of the triple-junction between the liquid film, the liquid substrate and the gas phase. The first approach is to incorporate an intermolecular potential which prevents that the film dewets completely. There will always remain a layer with height $h_* \ll 1$ which is called precursor. The second approach is to treat the triple-junction as a singular point (2D)/line (3D) and derive corresponding boundary conditions.

#### Thin-film model with precursor

A complete derivation of the model we are going to present here is found in [7]. Lets assume an arbitrary but fixed domain $\omega \subset \mathbb{R}^{d-1}$. In this domain we define $h_1, h : \{(x, y) \in \omega, t \geq 0\} \to \mathbb{R}^+$ as the thickness of the liquid substrate and the liquid film, e.g. see figures 1,2. They fulfill

the coupled system of degenerate fourth order parabolic equations

$$\partial_t h_1 = \nabla \cdot (Q_{11}\nabla\pi_1 + Q_{12}\pi_2)\,, \tag{1a}$$
$$\partial_t h = \nabla \cdot (Q_{21}\nabla\pi_1 + Q_{22}\pi_2)\,, \tag{1b}$$

with mobility matrix

$$Q = \frac{1}{\mu}\begin{pmatrix} \frac{1}{3}h_1^3 & \frac{1}{2}h_1^2 h \\ \frac{1}{2}h_1^2 h & \frac{\mu}{3}h^3 + h_1 h^2 \end{pmatrix}, \tag{1c}$$

and generalized pressures

$$\pi_1 = -(\sigma_1+\sigma_2)\Delta h_1 - \sigma_2\Delta h, \tag{1d}$$
$$\pi_2 = -\sigma_2\Delta h_1 - \sigma_2\Delta h + V_\varepsilon'(h). \tag{1e}$$

The constant $\mu$ denotes the viscosity-ratio between liquid substrate and the liquid film, while $\sigma_1$ is the surface tension at the liquid-liquid interface and $\sigma_2$ the one at the liquid-gas interface. As mentioned above this model contains an intermolecular potential which is given by

$$V_*(h) = \frac{h_*^8}{8h^8} - \frac{h_*^2}{2h^2} + 1. \tag{1f}$$

Models of this type are very popular in this field, e.g. [9, 15]. The reason is that due to the intermolecular potential one can usually avoid dealing with the degeneracy of the equation as $h \to 0$. Secondly, this approach has the advantage that it allows for quasi-topological transitions, in the sense that we have the transition from a wet substrate $h = \mathcal{O}(1)$ to a dry substrate $h = \mathcal{O}(h_*)$. A disadvantage of such models is that for $h_* \to 0$ second and higher order derivatives become unbounded and therefore require robust spatial and temporal adaptivity. To emphasize the dependence on the parameter $h_*$ we will henceforth write $h_1^*, h^*$ and refer to the model as *precursor model*.

**Thin-film model with triple-junction**

Here, we recall a model derived by Kriegsmann & Miksis [7]. In there intermolecular potentials are not used and therefore the thickness of the liquid film $h$ can be identically zero. That is why it is useful to divide $\omega$ into subregions. We denote by $\omega_0$ the region where the thickness of the upper liquid film is zero and by $\omega_+$ the region where it is greater than zero. Then obviously $\omega = \omega_0 \cup \omega_+$. Another consequence is that the evolution of the thickness of the liquid film $h$ can be described by a PDE only on $\omega_+$. Furthermore there are different PDEs for $h_1$ on $\omega_0$ and $\omega_+$. We set $h : \{x \in \omega_0, t \geq 0\} \to \mathbb{R}^+$ and $h_1|_{\omega_i} = h_{1,i} : \{x \in \omega_i, t \geq 0\} \to \mathbb{R}^+,\ (i \in \{0,+\})$. Then for $x \in \omega_0$

$$\partial_t h_{1,0} = -\partial_x\left(\frac{\sigma_1+\sigma_2}{3\mu}h_{1,0}^3\partial_x^3 h_{1,0}\right), \tag{2a}$$

and for $x \in \omega_+$ equations (1a) and (1b) hold but with $h_{1,+}$ instead of $h_1$ and new pressures

$$\pi_1 = -(\sigma_1+\sigma_2)\partial_x^2 h_{1,+} - \sigma_2\partial_x^2 h, \tag{2b}$$
$$\pi_2 = -\sigma_2\partial_x^2 h_{1,+} - \sigma_2\partial_x^2 h. \tag{2c}$$

The constant $\mu$ still denotes the viscosity ratio while $\sigma_1$ is the surface tension at the liquid-liquid interface and $\sigma_2$ the one at the liquid-gas interface in region $\omega_+$. In contrast to the precursor model we have an interior boundary $x_0 = \partial\omega_0 \cap \partial\omega_+$, the so-called triple-junction. Hence, the differential equations have to be equipped with boundary conditions at this point. The first two condition address the continuity of the profiles

$$h_{1,0} - h_{1,+} = 0, \qquad h = 0, \qquad \text{at } x = x_0. \tag{2d}$$

Next, we impose the contact angles at $x = x_0$ by

$$\begin{aligned} \partial_x h_{1,+} - \partial_x h_{1,0} &= -\sqrt{\frac{2\sigma\sigma_2}{\sigma_1(\sigma_1+\sigma_2)}}, \\ \partial_x h_{1,+} - \partial_x h_{1,0} + \partial_x h &= \sqrt{\frac{2\sigma\sigma_1}{\sigma_2(\sigma_1+\sigma_2)}}. \end{aligned} \tag{2e}$$

Here, $\sigma$ is the spreading coefficient. Furthermore, we wish to ensure continuity of the pressure in the liquid substrate and the velocity at $x = x_0$,

$$\pi_1 + (\sigma_1+\sigma_2)\partial_x^2 h_{1,0} = 0, \tag{2f}$$

$$\partial_x \pi_1 + (\sigma_1+\sigma_2)\partial_x^3 h_{1,0} = 0. \tag{2g}$$

Finally, we need one condition for the evolution of the contact point itself,

$$\frac{d}{dt}x_0(t) = \lim_{x \nearrow x_0} \left( \frac{\sigma_1+\sigma_2}{2\mu} h_{1,0}^2 \partial_x^3 h_{1,0} \right). \tag{2h}$$

The velocity can also be defined as a limit $x \searrow x_0$, or as an limit in terms of $h$. But there is a boundary condition which states that these limits are equal. In the remaining part of the paper we will refer to models where the triple-junction is treated explicitly as *sharp-interface models*. One aim of the next sections is to provide a suitable weak formulation for the model (2) and to compare its solutions with the ones to the precursor model (1).

# 2 Dynamics of viscous bilayers as gradient flows

In this section we derive a Stokes free-boundary problem for liquid bilayers and a corresponding PDE system for the corresponding thin-film approximation. Both liquids are immiscible, viscous and incompressible with a no-slip condition at the liquid interface as sketched in figure 1. The PDE will be derived using a gradient flow formulation.

The flow is driven by the surface energy and the shape of the interfaces depends on time and the triple-junctions are treated using a sharp-interface model. We want to emphasize that it is useful to use the gradient flow structure of the system in order to identify all boundary conditions needed for the derived systems. We refrain from showing the calculation behind the thin-film approximation, since this is rather standard and can be found elsewhere [7]. The concept of

gradient flow formulations in this class of models is well-known, e.g. works by Otto [16] or the recent study by Rumpf [17].

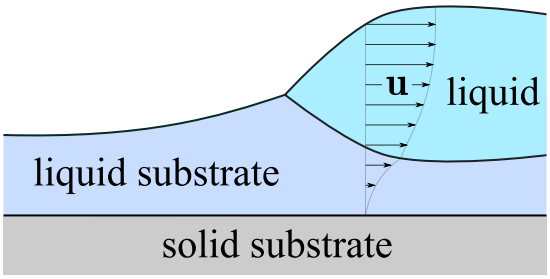


Figure 1: Flow of a liquid on a liquid substrate above a solid substrate, where both liquids meet the ambient gaseous phase in the triple-junction.

## 2.1 Stokes flow

Consider the free-surface flow of two viscous, immiscible liquids in the half-space $\Omega = \Omega_1(t) \cup \Omega_2(t) \subset \omega \times \mathbb{R}^+$ where $\omega \subset \mathbb{R}^{d-1}$. The dynamics is parameterized by the *continuous* flow map $\Psi_t$ with $\Omega_\ell(t) = \Psi_t\big(\Omega_\ell(0)\big)$ for $\ell = 1, 2$. Incompressibility implies that the velocity $\mathbf{u} := \partial_t \Psi_t$ obeys $\nabla \cdot \mathbf{u} = 0$. For fixed time assume that the domains can be parameterized by functions $h_1(t, \circ), h(t, \circ) : \omega \to \mathbb{R}$ as follows

$$\begin{aligned}\Omega_1(t) &:= \{(x, z) \in \omega \times \mathbb{R}^+ : 0 < z < h_1(t, x)\},\\ \Omega_2(t) &:= \{(x, z) \in \omega \times \mathbb{R}^+ : h_1(t, x) < z < h_1(t, x) + h(t, x)\},\end{aligned}$$

and restrict to situations where $0 < h_1 \leq h_1 + h$. For ease of notation assume that we are in $d = 2$ and have $\omega = (0, L)$. Then let $0 < x_- < x_+ < L$ given and define

$$\omega_1 = \big(0, x_-\big), \quad \omega_2 = \big(x_-, x_+\big), \quad \omega_3 = \big(x_+, L\big).$$

We have the free interfaces

$$\begin{aligned}&\text{liquid 1-liquid 2:} && \Gamma_1 = \{(x, z) : x \in \omega_2, z = h_1(t, x)\}\\ &\text{liquid 2-gas:} && \Gamma_2 = \{(x, z) : x \in \omega_2, z = h_1(t, x) + h(t, x)\}\\ &\text{liquid 1-gas:} && \Gamma_3 = \{(x, z) : x \in (\omega_1 \cup \omega_2), z = h_1(t, x)\}\end{aligned}$$

and triple-points at $\{x, z\} = \{x_\pm(t), h_1(t, x_\pm)\}$. This constitutes a typical droplet-like configuration as it is also shown in figure 2.

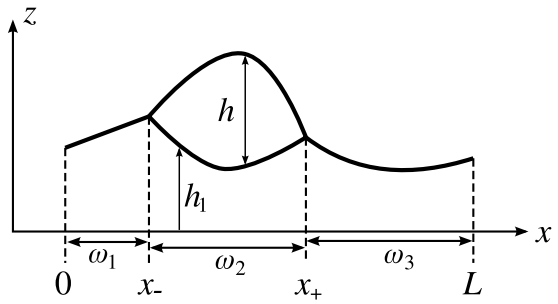


Figure 2: Sketch of geometry

Since early works of Rayleigh, Helmholtz and Korteweg it is known that viscous flows minimize the dissipation of energy [18]. For given initial domains $\Omega_1, \Omega_2$ the key ingredients to construct the PDE formulation from a variational principle are the energy

$$E(\Psi_t) := \sum_{j=1}^{3} \int_{\Psi_t(\Gamma_j(0))} \gamma_j \, d\Gamma \, . \tag{3}$$

where $\gamma_j$ specifies the amount of energy carried by $\Gamma_j(t)$ per unit area. The dissipation $D$ is defined as the energy per time to change a state with velocity $\mathbf{u}$ and for Newtonian liquids it is given by

$$D = \sum_{\ell=1}^{2} \frac{\mu_\ell}{4} \int_{\Omega_\ell(t)} (\nabla \mathbf{u} + \nabla \mathbf{u}^\top)^2 \, d\Omega \, . \tag{4}$$

Solutions of the Stokes flow $\Psi_t$ satisfy the variational principle

$$\tfrac{d}{dt}\Psi_t = \operatorname{argmin}_{\mathbf{u}} \left( \tfrac{1}{2} D(\mathbf{u}, \mathbf{u}) + \langle \operatorname{diff} E(\Psi_t), \mathbf{u} \rangle \right) , \tag{5}$$

which is formally equivalent to writing $\partial_t \Psi_t = -\nabla_D E(\Psi_t)$. The variational principle requires the calculation of

$$\langle \operatorname{diff} E, \mathbf{v} \rangle = - \sum_{j=1}^{3} \gamma_j \left( (d-1) \int_{\Gamma_j} \kappa \mathbf{n} \cdot \mathbf{v} \, d\Gamma - \mathbf{v} \cdot \mathbf{n}_{\Gamma_j} \Big|_{x_-, x_+} \right) \tag{6}$$

which is evaluated at $t = 0$ where $\Psi_t = \mathrm{id}_\Omega$. The necessary condition for (5) is that $D(\mathbf{u}, \mathbf{v}) = -\langle \operatorname{diff} E(\Psi_t), \mathbf{v} \rangle$ for all admissible test-velocities $\mathbf{v}$. Using integration by parts and $\tau_\ell = \mu_\ell (\nabla \mathbf{u} + \nabla \mathbf{u}^\top)$ gives

$$\begin{aligned} -\sum_{\ell=1}^{2} \int_{\Omega_\ell} \big(\nabla \cdot \tau_\ell\big) \mathbf{v} \, d\Omega + \int_{\cup \Gamma_j} \mathbf{v} \cdot \left( [[\tau]] \mathbf{n} - (d-1) \gamma_j \kappa \mathbf{n} \right) d\Gamma \\ + \quad \sum_j \mathbf{v} \cdot \gamma_j \mathbf{n}_{\Gamma_j} \Big|_{\{x_\pm, h(t, x_\pm)\}} = 0 \end{aligned} \tag{7}$$

with the $[[\tau]]\mathbf{n} = (\tau_2 - \tau_1)\mathbf{n}$ denoting the jump across the interface. Since each term vanishes separately we get $\nabla \cdot \tau = 0$ in $\Omega_l$, $[[\tau]]\mathbf{n} = (d-1)\gamma_j \mathbf{n}$ on $\Gamma_j$, and the Neumann triangle condition [19] stating $\gamma_1 \mathbf{n}_{\Gamma_1} + \gamma_2 \mathbf{n}_{\Gamma_2} + \gamma_3 \mathbf{n}_{\Gamma_3} = 0$ at triple junctions $\{x_\pm, h_1(t, x_\pm)\}$. This formulation is equivalent to the one used by Kriegsmann [7] as the basis for the further thin-film approximation.

In order to perform a thin-film approximation in the energy $E$ one can rewrite

$$E(\Psi_t) \equiv E(h_1, h) = \int_\omega \sigma_1(x)\sqrt{1 + |\nabla h_1|^2} + \sigma_2(x)\sqrt{1 + |\nabla(h_1 + h)|^2}\,\mathrm{d}x.$$

where

$$\sigma_1(x) = \begin{cases} \gamma_1 & x \in \omega_2, \\ \gamma_3 - C & \text{else}, \end{cases} \qquad \sigma_2(x) = \begin{cases} \gamma_2 & x \in \omega_2, \\ C & \text{else}. \end{cases}$$

where we have introduced an arbitrary constant $C$ since $h = 0$ on $\omega_1 \cup \omega_3$.

A small-slope approximation $[h] = \varepsilon[x]$ of $E$ in powers of $\varepsilon$ gives

$$E = \int_\omega \sigma_1(x) + \sigma_2(x) + \varepsilon^2 \left( \tfrac{\sigma_1(x)}{2}|\nabla h_1|^2 + \tfrac{\sigma_2(x)}{2}|\nabla(h_1 + h)|^2 \right) \mathrm{d}x + \mathcal{O}(\varepsilon^4)$$

To balance the nontrivial leading order terms we expand $\gamma_i = \gamma_i^0 + \gamma_i^1 \varepsilon^2 + O(\varepsilon^4)$ and get $\gamma_1^0 + \gamma_2^0 - \gamma_3^0 = 0$. Then the next order is

$$\varepsilon^{-2}\big(E + o(1)\big) = F(h_1, h) := \int_\omega \frac{\sigma_1}{2}|\nabla h_1|^2 + \frac{\sigma_2}{2}|\nabla(h_1 + h)|^2 + \sigma(x)\,\mathrm{d}x \tag{8}$$

where with $C = \gamma_2^0$ we get

$$\begin{aligned} &\sigma_1 = \gamma_1^0, \\ &\sigma_2 = \gamma_2^0, \\ &\sigma(x) = (-\sigma)\chi\{h > 0\} = \begin{cases} -\sigma & x \in \omega_2 \\ 0 & \text{else} \end{cases} \end{aligned}$$

with spreading coefficient $\sigma = \gamma_3^1 - \gamma_1^1 - \gamma_2^1$. In a dewetting scenario we have $\sigma < 0$. To leading order in $\varepsilon$ we have that $F$ in (8) is equivalent to $E$. A similar line of arguments has been used by Kriegsmann and Miksis in [7]. Now we are going to construct a thin-film gradient flow based on the energy $F$.

## 2.2 Thin-film flow

As before we have $\Omega_1, \Omega_2$ defined by functions $h_1 : \omega \to \mathbb{R}$ and $h : \omega_2 \to \mathbb{R}$ where $h_1$ is continuous and $h$ has zero boundary conditions at $x_-$ and $x_+$. One can extend $h : \omega \to \mathbb{R}$ by zero. Furthermore, the volumes

$$m_1(t) = \int_\omega h_1(t, x)\,\mathrm{d}x, \qquad m_2(t) = \int_\omega h(t, x)\,\mathrm{d}x$$

are conserved $m_1(t) = M_1$ and $m_2(t) = M_2$. These conditions formally define a manifold

$$\begin{aligned}\mathcal{M} \;=\; \Big\{&\{h_1, h, x_-, x_+\} : \{x : h(x) > 0\} = (x_-, x_+), 0 < x_- < x_+ < L,\\ &m_1(t) = M_1, \quad m_2(t) = M\Big\}\end{aligned}$$

so that a solution is a curve $\mathbf{s}(t) := \{h_1(t,\cdot), h(t,\cdot), x_-(t), x_+(t)\} \in \mathcal{M}$. Provided that $\mathbf{s}(t) = \{h_1(t,\circ), h(t,\circ), x_-(t), x_+(t)\}$ is differentiable in time and sufficiently smooth in space one immediately derives the condition

$$\frac{d}{dt} h\big(t, x_\pm(t)\big) = 0$$

from $h\big(t, x_\pm(t)\big) = 0$. Then this implies that changes $\dot{h}$ and $\dot{x}_\pm$ are not independent but related by

$$\begin{aligned}\dot{h}(t, x_-) + \dot{x}_- \cdot \nabla h(t, x_-) = 0,\\ \dot{h}(t, x_+) + \dot{x}_+ \cdot \nabla h(t, x_+) = 0,\end{aligned} \tag{9a}$$

where we used the notation $\dot{h}(t,x) := \partial_t h(t,x)$ and $\dot{x}_\pm := dx_\pm/dt$. Furthermore

$$\begin{aligned}\lim_{\varepsilon \searrow 0} \frac{d}{dt} h_1\big(t, x_-(t) + \varepsilon\big) &= \lim_{\varepsilon \nearrow 0} \frac{d}{dt} h_1\big(t, x_-(t) + \varepsilon\big)\\ \lim_{\varepsilon \searrow 0} \frac{d}{dt} h_1\big(t, x_+(t) + \varepsilon\big) &= \lim_{\varepsilon \nearrow 0} \frac{d}{dt} h_1\big(t, x_+(t) + \varepsilon\big)\end{aligned}$$

which again implies

$$\begin{aligned}[[\dot{h}_1 + \dot{x}_- \cdot \nabla h_1]]_{x_-} = 0\\ [[\dot{h}_1 + \dot{x}_+ \cdot \nabla h_1]]_{x_+} = 0\end{aligned} \tag{9b}$$

with the notation $[[g]]_{x_\pm} = \lim_{x \nearrow x_\pm} g(x) - \lim_{x \searrow x_\pm} g(x)$ to express the jump of a quantity across $x_\pm$.

The tangent space $\mathrm{T}_{\mathbf{s}}\mathcal{M}$ is characterized by velocities $\dot{\mathbf{s}} = \{\dot{h}_1, \dot{h}, \dot{x}_-, \dot{x}_+\}$ of curves $\mathbf{s}(t)$ in $\mathcal{M}$. Note that even on this entirely formal level that $\mathcal{M}$ is not a linear space. If for $\mathbf{s}, \tilde{\mathbf{s}} \in \mathcal{M}$ the corresponding $x_\pm, \tilde{x}_\pm$ are different, then $h$ and $\tilde{h}$ have different supports and thereby $h + \tilde{h}$ is meaningless. We define formally a metric $d_{\mathbf{s}} : \mathrm{T}_{\mathbf{s}}\mathcal{M} \times \mathrm{T}_{\mathbf{s}}\mathcal{M} \to \mathbb{R}$ as follows. First define the auxiliary pressures $\pi_1,\ \pi_2 \in H^1(\omega)$ as weak solutions of

$$\int_\omega \dot{h}_1 \phi_1 + (Q_{11}\nabla\pi_1 + Q_{12}\nabla\pi_2)\nabla\phi_1 \,\mathrm{d}x = 0, \tag{10a}$$

$$\int_{\omega_2} \dot{h}\phi + (Q_{21}\nabla\pi_1 + Q_{22}\nabla\pi_2)\nabla\phi \,\mathrm{d}x = 0, \tag{10b}$$

considered with a symmetric matrix for $h_1, h > 0$

$$Q_{ij} = \frac{1}{\mu}\begin{pmatrix} \frac{1}{3}h_1^3 & \frac{1}{2}h_1^2 h \\ \frac{1}{2}h_1^2 h & \frac{\mu}{3}h^3 + h_1 h^2 \end{pmatrix}.$$

The definition of $\pi_i$ implies that the flux $J_i = Q_{ij}\nabla\pi_j$ is zero at $x = \{0, L\}$, $[[J_1]] = 0$ and $J_2 = 0$ at $x_\pm$, which basically implies conservation of masses $\dot{m}_1 = \dot{m}_2 = 0$. As in the previous section $\mu = \mu_1/\mu_2$ is the ratio of the viscosities. Note that $\dot{h}_1$ jump at $x_\pm$ but $\pi_1$ is continuous. The pressure $\pi_2$ is only well defined on $\omega_2$. Both pressures $\pi_i$ are only defined up to an additive constant, which we fix by requiring

$$\int_\omega \pi_1 \,\mathrm{d}x = \int_{\omega_2} \pi_2 \,\mathrm{d}x = 0.$$

Now we define the metric as follows

$$d_{\mathbf{s}}(\dot{\mathbf{s}}, \dot{\mathbf{s}}) = \sum_{i,j=1}^{2} \int Q_{ij}\nabla\pi_i\nabla\pi_j \,\mathrm{d}x. \tag{11}$$

As $\{\pi_1, \pi_2\}$ depend linearly on $\{\dot{h}_1, \dot{h}, \dot{x}_-, \dot{x}_+\}$ by (10) it follows that (11) defines a symmetric positive definite bilinear form. Let us further consider the energy $F : \mathcal{M} \to \mathbb{R}$

$$F(h_1, h) = \int_\omega e(x, h_1, h) \,\mathrm{d}x$$

where $e$ is the abbreviation for

$$e(x, h_1, h) := \frac{\sigma_1}{2}|\nabla h_1|^2 + \frac{\sigma_2}{2}|\nabla(h_1 + h)|^2 + \sigma(x).$$

The Rayleigh principle applied to $F$ considered with the metric (11) implies that for a solution curve $\mathbf{s}(t) = \{h_1(t,\cdot), h(t,\cdot), x_-(t), x_+(t)\}$ the velocity $\dot{\mathbf{s}}(t) = \{\dot{h}_1(t,\cdot), \dot{h}(t,\cdot), \dot{x}_-(t), \dot{x}_+(t)\}$ solves the following variational problem

$$\dot{\mathbf{s}}(t) = \mathrm{argmin}_{\dot{\tilde{\mathbf{s}}}\in \mathrm{T}_{\mathbf{s}}\mathcal{M}} \left( \frac{1}{2} d_{\mathbf{s}}(\dot{\tilde{\mathbf{s}}}, \dot{\tilde{\mathbf{s}}}) + \mathrm{diff} F(\mathbf{s})[\dot{\tilde{\mathbf{s}}}] \right),$$

or alternatively $\dot{\mathbf{s}}$ fulfills

$$d_{\mathbf{s}}(\dot{\tilde{\mathbf{s}}}, \dot{\mathbf{s}}) = -\mathrm{diff} F(\mathbf{s})[\dot{\tilde{\mathbf{s}}}], \qquad \forall\, \dot{\tilde{\mathbf{s}}} \in \mathrm{T}_{\mathbf{s}}\mathcal{M}. \tag{12}$$

In other words we defined the gradient $\dot{\mathbf{s}} = -\nabla_d F(\mathbf{s})$. This is the basic weak formulation, which we will use in the next section to compute numerical solution. There we will propose a definition of a time-step in $\mathcal{M}$ which is compatible with its nonlinear structure.

Next in this section it remains to formally identify the gradient, so that we are able to compare with the well-known PDE formulation of bilayer flows. Therefore we perform integration by parts in the metric

$$\begin{aligned} d_{\mathbf{s}}(\dot{\mathbf{s}}, \dot{\tilde{\mathbf{s}}}) &= \int_\omega Q_{ij}\nabla\pi_j\nabla\tilde{\pi}_i \,\mathrm{d}x \\ &= \int_\omega -\nabla\cdot\big(Q_{ij}\nabla\tilde{\pi}_i\big)\pi_j \,\mathrm{d}x \\ &= \int_\omega -(\dot{\tilde{h}}_1\pi_1 + \dot{\tilde{h}}\pi_2) \,\mathrm{d}x \end{aligned}$$

and in the derivative of the energy

$$\begin{aligned}\mathrm{diff}F(\mathbf{s})[\tilde{v}] &= \int_\omega \sigma_1 \nabla h_1 \nabla \dot{\tilde{h}}_1 + \sigma_2(\nabla h_1 + \nabla h)(\nabla \dot{\tilde{h}}_1 + \nabla \dot{\tilde{h}})\mathrm{d}x + \int_{\partial\omega} e\,\dot{\tilde{x}} \cdot \mathbf{n} \\ &= -\int_\omega \sigma_1 \Delta h_1 \dot{\tilde{h}}_1 + \sigma_2(\Delta h_1 + \Delta h)(\dot{\tilde{h}}_1 + \dot{\tilde{h}})\mathrm{d}x + \int_{\partial\omega} [[e+b]]\,\dot{\tilde{x}} + [[c]]\dot{\tilde{H}}_1.\end{aligned}$$

The term $b := -\sigma_1|\nabla h_1|^2 - \sigma_2|\nabla(h_1+h)|^2$ comes from integration by parts using (9) and $c := \sigma_1\nabla h_1 + \sigma_2\nabla(h_1+h)$. Using the above transformations and (12) one finds that up to an additive constant

$$\begin{aligned}\pi_1 &= -(\sigma_1+\sigma_2)\Delta h_1 - \sigma_2 \Delta h \\ \pi_2 &= -\sigma_2(\Delta h_1 + \Delta h)\end{aligned} \tag{13}$$

hold in $\omega$ and $\omega_2$ respectively. Since $\dot{\tilde{x}}$, $\dot{\tilde{H}}_1 := \dot{\tilde{h}}_1 + \dot{\tilde{x}} \cdot \nabla h_1$ can be varied independently we get

$$[[e+b]] = 0, \qquad [[c]] = 0 \qquad \text{at } x = x_\pm \tag{14}$$

A simple calculation shows that these conditions are equivalent to (2e). Finally, one obtains a closed PDE system for $h_1(t,x), h(t,x), x_-(t), x_+(t)$

$$\begin{aligned}\dot{h}_1 - \nabla \cdot (Q_{11}\nabla\pi_1 + Q_{12}\nabla\pi_2) &= 0 \\ \dot{h} - \nabla \cdot (Q_{21}\nabla\pi_1 + Q_{22}\nabla\pi_2) &= 0\end{aligned} \tag{15}$$

combined with (13), the boundary conditions prescribed by (14) and the conservation of masses $m_1(t) = M_1$ and $m_2(t) = M_2$. Note that in $\omega_1 \cup \omega_3$ we have $Q_{12} = Q_{21} = Q_{22} = 0$ and thereby

$$\dot{h}_1 + \nabla \cdot \left( \frac{(\sigma_1+\sigma_2)h_1^3}{3\mu} \nabla \Delta h_1 \right) = 0, \qquad \dot{h} = 0, \tag{16}$$

which is the standard thin-film equation for a single layer of height $h_1$. Thereby, the derived gradient system coincides with the PDE formulation as introduced by Kriegsmann [7].

# 3 Numerical algorithm

Let us consider the gradient formulation as stated before in the form

$$d_{\mathbf{s}}(\dot{\tilde{\mathbf{s}}}, \dot{\mathbf{s}}) = -\mathrm{diff}F(\mathbf{s})[\dot{\tilde{\mathbf{s}}}], \qquad \forall\, \dot{\tilde{\mathbf{s}}} \in \mathrm{T}_{\mathbf{s}}\mathcal{M},$$

and suppose that we have already discretized $h, h_1$ e.g. using $\mathbb{P}_1$ finite elements. As it was noticed before $\dot{h}, \dot{h}_1$ are not continuous across $x_\pm$, and obey certain linear constraints (9) which define the tangent space $\mathrm{T}_{\mathbf{s}}\mathcal{M}$. It might be generally difficult to enforce all these linear constraints $C\mathbf{s} = 0$ explicitly. Therefore we seek solutions $\dot{\mathbf{s}}$ in a larger space $V_h$ and enforce the conditions using Lagrange multipliers, i.e. seek $\dot{\mathbf{s}} \in V_h$ such that

$$d_{\mathbf{s}}(\dot{\mathbf{s}}, \dot{\tilde{\mathbf{s}}}) + < \dot{\tilde{\mathbf{s}}}, C^\top \lambda > = -\mathrm{diff}F(\mathbf{s})[\dot{\tilde{\mathbf{s}}}] \tag{17}$$

$$< \tilde{\lambda}, C\dot{\mathbf{s}} > = 0 \tag{18}$$

for all $\dot{\tilde{\mathrm{s}}} \in V_h$ and multiplier $\tilde{\lambda}$. Please note that each constraint is accompanied by a term $C^\top$ which consistently couples the multiplier to the actual problem. Rows of the constraint matrix $C$ explicitly include the discretized weak form of

$$\begin{aligned} \int_\omega \dot{h}_1\phi_1 + (Q_{11}\nabla\pi_1 + Q_{12}\nabla\pi_2)\nabla\phi_1 \,\mathrm{d}x = 0 \\ \int_{\omega_2} \dot{h}\phi_2 + (Q_{21}\nabla\pi_1 + Q_{22}\nabla\pi_2)\nabla\phi_2 \,\mathrm{d}x = 0 \end{aligned} \tag{19}$$

for all $\phi_1, \phi_2$. Furthermore $C$ contains pointwise evaluations of

$$\begin{aligned} \dot{h}(t, x_-) + \dot{x}_- \cdot \nabla h(t, x_-) = 0, \\ \dot{h}(t, x_+) + \dot{x}_+ \cdot \nabla h(t, x_+) = 0, \\ [[\dot{h}_1 + \dot{x}_- \cdot \nabla h_1]]_{x_-} = 0, \\ [[\dot{h}_1 + \dot{x}_+ \cdot \nabla h_1]]_{x_+} = 0. \end{aligned}$$

In addition we have the two scalar constraints

$$\begin{aligned} \int_\omega \pi_1 \mathrm{d}x = 0 \\ \int_{\omega_2} \pi_2 \mathrm{d}x = 0 \end{aligned}$$

In order to construct $V_h$ we use $\mathbb{P}_1$ finite element functions

$$\dot{h}_1 = \sum_{i=1}^{N_\varphi} \dot{h}_1^i \varphi_i(x), \qquad\qquad \dot{h} = \sum_{i=1}^{N_\chi} \dot{h}^i \chi_i(x),$$

where $\varphi$ might jump at $x_\pm$ so that there is a double-counting of degrees of freedoms. Since $\dot{h}$ is only defined on $\omega_2$, the same properties holds for $\chi_i$. The auxially variable $\pi_1$ is continuous and $\pi_2$ is only defined on $\omega_2$. The same holds for holds for the functions $\phi_1, \phi_2$ in (19). The time-discretization is via a semi-implicit Euler method in the way that we replaced $\{h_1, h\} \to \{h_1 + \tau\dot{h}_1, h + \tau\dot{h}\}$ in $\mathrm{diff}F$ as mentioned before.

Finally this leads to a discrete problem, where we seek solutions

$$\{\dot{h}_1, \dot{h}, \pi_1, \pi_2, \dot{x}, \dot{x}_+, \dot{x}_-, \lambda\}$$

where the $\pi_i$ appear explicitly and $\lambda$ are the Lagrange multiplier for the constraint $C$. As in the introduction is makes sense to define the restrictions

$$\dot{h}_{1,k} = \dot{h}_1\Big|_{\omega_k}, \qquad\qquad \dot{h}_{0,k} = \dot{h}\Big|_{\omega_k}.$$

The corresponding counting of degrees of freedom for a small mesh with 8 nodes is illustrated in figure 3. Note again that $\dot{h}_1$ is discontinuous, $\pi_1$ is continuous, and $\dot{h}$ is defined on $\omega_2$ with nonzero boundary values.

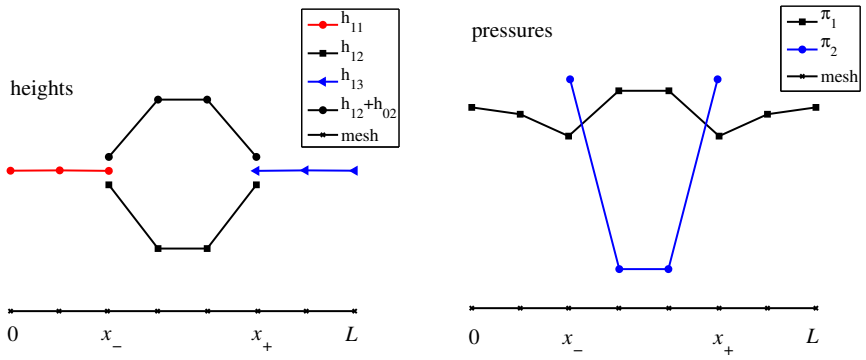


Figure 3: Sketch of discrete degrees of freedom $\dot{h}_1, \dot{h}$ (left) and $\pi_1, \pi_2$ (right) on a coarse mesh of 8 points.

Using these definitions our weak formulation $d(\mathbf{s}, \circ) = -\mathrm{diff} F(\circ)$ can be written in a block-form as follows

$$\left(\begin{array}{c|cc|c} \tau(\sigma S) & & & \\ \hline & Q_{11}S & Q_{12}S & \\ & Q_{21}S & Q_{22}S & \\ \hline & & & \end{array}\right) \left(\begin{array}{c} \dot{h}_{11} \\ \dot{h}_{12} \\ \dot{h}_{13} \\ \dot{h}_{02} \\ \hline \dot{\pi}_1 \\ \dot{\pi}_2 \\ \hline \dot{x}_- \\ \dot{x}_+ \end{array}\right) = \left(\begin{array}{c} -(\sigma S)h_{11} \\ -(\sigma S)h_{12} \\ -(\sigma S)h_{13} \\ -(\sigma S)h_{02} \\ \hline 0 \\ 0 \\ \hline +e(x_-) \\ -e(x_+) \end{array}\right) \tag{20}$$

where blank blocks are zero. We used the following abbreviations

$$\langle \tilde{v}, \sigma S v \rangle = \int_\omega \sigma_1 \nabla \dot{h}_1 \nabla \dot{\tilde{h}}_1 + \sigma_2 (\nabla \dot{h}_1 + \nabla \dot{h})(\nabla \dot{\tilde{h}}_1 + \nabla \dot{\tilde{h}}) \mathrm{d}x$$

which appears in the matrix with a factor of $\tau$ after replacing $h_1 \to h_1 + \tau \dot{h}_1$ and $h \to h + \tau h$ in $\delta F_{h,h_1}[\tilde{v}]$ to make the corresponding derivative semi-implicit. Furthermore we have

$$\langle \tilde{v}, Q_{ij} S\, v \rangle = \int_\omega Q_{ij} \nabla \pi_i \nabla \tilde{\pi}_j \,\mathrm{dx}$$

with the noted properties on the domain of definition of $\pi_j$. Plugging in the local definition we obtain for instance

$$\langle \tilde{v}, Q_{11} S\, v \rangle = \left( \int_{\omega_1 \cup \omega_3} \frac{h_1^3}{3\mu} \nabla \psi_i \nabla \psi_j \mathrm{d}x \right) \pi_1^i \tilde{\pi}_1^j$$

Once we have computed $\dot{\mathbf{s}}$ the question is how we are using it to compute a new solution? One clearly should *not* update $h(t+\tau, x) = h(t,x) + \tau \dot{h}(x)$ since this readily violates the boundary condition $h(t, x_\pm) = 0$. As we mentioned earlier the solution manifold is not linear. What one

should rather do is define an extension of the velocities $\dot{x}_\pm$ onto the domain $\omega$, e.g. by setting

$$\dot{\xi}(x) := \begin{cases} \dot{x}_- \frac{x}{x_-} & x \in \omega_1 \\ \dot{x}_- \left(1 - \frac{x-x_-}{x_+-x_-}\right) + \dot{x}_+ \left(\frac{x-x_-}{x_+-x_-}\right) & x \in \omega_2 \\ \dot{x}_+ \left(1 - \frac{L-x}{L-x_+}\right) & x \in \omega_3 \end{cases} \tag{21}$$

with the obvious properties $\dot{\xi}(0) = \dot{\xi}(L) = 0$, $\dot{\xi}(x_\pm) = \dot{x}_\pm$. The mapping $\xi(x)$ is equidistant in each $\omega_i$, i.e. $\partial_x \xi = C_i > 0$ in each $\omega_i$ as long as we have $0 < x_-(t) < x_+(t) < L$. If the corresponding flow map is $\xi_t(x) := x + \int_0^t \dot{\xi}(x)\,\mathrm{d}t$ then one can easily see that with $H(t,x) = h\big(t, \xi_t(x)\big)$ we have

$$\dot{h}(t,x) + \dot{\xi}(x) \cdot \nabla h(t,x) = \dot{H}(t,x)$$
$$\dot{h}_1(t,x) + \dot{\xi}(x) \cdot \nabla h_1(t,x) = \dot{H}_1(t,x)$$

where $\dot{H}$ has zero boundary conditions and $\dot{H}_1$ is continuous at $x_\pm$. Now we can update the Lagrangian coordinates via

$$\xi_{t+\tau}(x) = x + \tau \dot{\xi}(x), \tag{22a}$$
$$H(t+\tau, x) = h(t,x) + \tau \dot{H}(t,x), \tag{22b}$$
$$H_1(t+\tau, x) = h_1(t,x) + \tau \dot{H}_1(t,x). \tag{22c}$$

so that $h(t+\tau, \xi_{t+\tau}(x)) := H(t+\tau, x)$ and $h_1(t+\tau, \xi_{t+\tau}(x)) := H_1(t+\tau, x)$. This is the final step of the numerical algorithm. Using the map $\xi$ guarantees that solutions never leave the manifold. We check the robustness of the algorithm with respect to temporal and spatial discretization for one example.

**Example 3.1.** Consider the initial data on $\omega = [0, 8]$ with $x_-(0) = 3$ and $x_+(0) = 5$

$$h_1(0,x) = 1, \qquad h(0,x) = (1 - |4 - x|)_+$$

with $\tau = 1/n_t$ and $\delta x = |\omega_i|/n_x$ in each $\omega_i$. As parameters for this example we choose

$$\sigma_1 = 1, \qquad \sigma_2 = 1, \qquad \sigma(x) = \begin{cases} 1 & x \in \omega_2 \\ 0 & \text{else} \end{cases}.$$

The corresponding solution $h_1, h$ are shown in figure 4. Each domain is discretized separately, e.g. for $\omega_1$ we have $0 = x_1 < \ldots < x_{N_p} = x_-$ with corresponding standard finite element space. Figure 4 shows the dependence of the solution at $t = 1$. Note that the initial data is not smooth at $x = 4$, still solutions with different $n_t$ roughly agree even for $n_t = 1$. For $n_t \to \infty$ we see typical convergence for a first order method. It seems that at $t \to 0$ there is some loss of volume $m_1, m_2$ which might be due to the fact the initial data do not satisfy the equilibrium conditions $[[e + b]] = 0$, $[[c]] = 0$. Similarly the method is quite robust when using coarse meshes with as few as $N_p = 5$ points for each interval $\omega_i$. This is particularly interesting for applications of the numerical algorithm in $d = 3$.

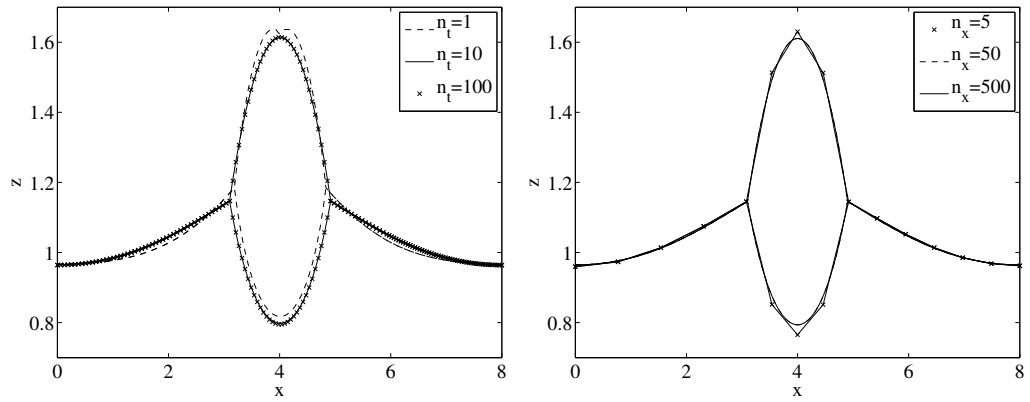


Figure 4: Convergence of solution $(h_1, h, x_-, x_+)$ at time $t = 1$ depending on number of time-steps $n_t$ (left) or spatial discretization $n_s$ (right).

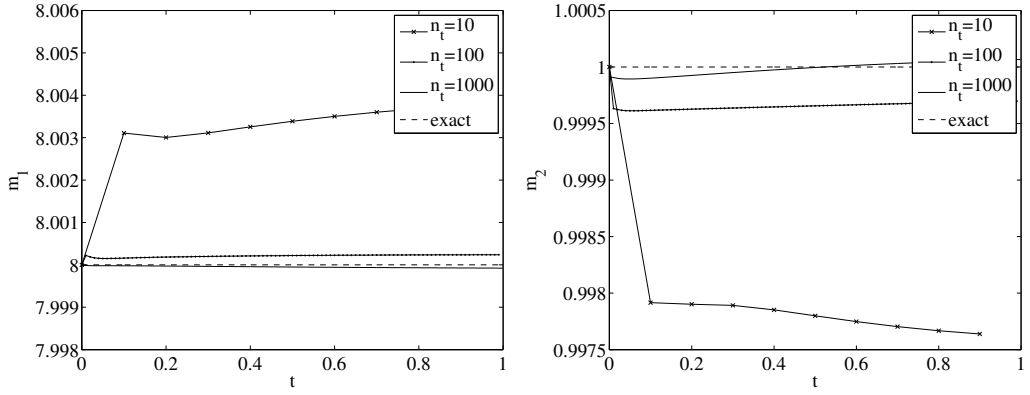


Figure 5: Convergence mass $m_1, m_2$ as a function of time depending on time-discretization.

In what follows we will also compare the gradient approach with numerical solutions of (1). Corresponding algorithms for thin-film equations with precursor are rather standard and have been discussed throughout the literature. Our implementation uses a fully-implicit time-discretization and second finite-differences in space. Time-step size is adaptively refined using step-size bisection and a Richardson extrapolation.

# 4 Validation of gradient model

In this section we are going to compare the numerical solutions of the gradient formulation with other solutions of thin-film bilayer systems. First we compare solutions to solutions of a bilayer systems with precursor and then we compare with an asymptotically exact source-type solutions for a spreading droplet on a liquid substrate with $\sigma(x) \equiv 0$.

## 4.1 Comparison with precursor model

Consider the precursor energy

$$F_*(h_1, h) = \int_\omega \frac{\sigma_1}{2}|\nabla h_1|^2 + \frac{\sigma_2}{2}|\nabla h_1 + h|^2 + \sigma V_*(h)\,\mathrm{d}x$$

corresponding to the model (1), where $h_*$ is a small positive parameter controlling the minimum thickness of $h$. Using $\pi_1 = \delta F_*/\delta h_1$ and $\pi_2 = \delta F_*/\delta h$ gives the formulation (1) from section 1. Stationary solutions of (1) are known to minimize $F_*$ subject to the constraint that we keep the mass fixed, i.e.,

$$\{h_1^*, h^*\} = \mathrm{argmin}_{\mathcal{X}}\, F_*$$

where $\mathcal{X} = \{(h_1, h) \in H^1(\omega)^2, m_1 = M_1, m_2 = M_2, h_1 > 0, h \geq 0\}$. Limiting properties of such a sequence of minimizers $\{h_1^*, h^*\}_{h_*}$ can be shown in the framework of $\Gamma$-convergence. In a previous paper we showed that

$$\Gamma\text{-}\lim_{h_*\to 0} F_* = \int_\omega \frac{\sigma_1}{2}|\nabla h_1|^2 + \frac{\sigma_2}{2}|\nabla h_1 + h|^2 + \sigma\chi\{h > 0\}\,\mathrm{d}x \equiv F$$

i.e., roughly speaking we have that $\{h_1^*, h^*\}_{h_*}$ (weakly) converge as $h_* \to 0$ and the limit minimizes $F$. Using an rearrangement argument we rigorously showed that minimizers of $F$ are liquid lenses

$$h_1(x) = \hat{H}_1 - \rho(\hat{H}_0 - |x - x_0|^2)_+$$
$$h(x) = \kappa(\hat{H}_0 - |x - x_0|^2)_+$$

with for $\hat{H}_0, \hat{H}_1, \rho, \kappa \in \mathbb{R}^+$ determined by the constraints $[[e + b]] = 0, [[c]] = 0, m_1 = M_1$, $m_2 = M_2$ and $x_0 \in \omega \subset \mathbb{R}^{d-1}$ arbitrary. To keep the proof this general we had to work with balls $\omega = B_r$ and then we need to choose $x_0$ so that $\{h > 0\} \subset \omega$. A typical stationary solution from the precursor model and the gradient model are shown in figure 6.

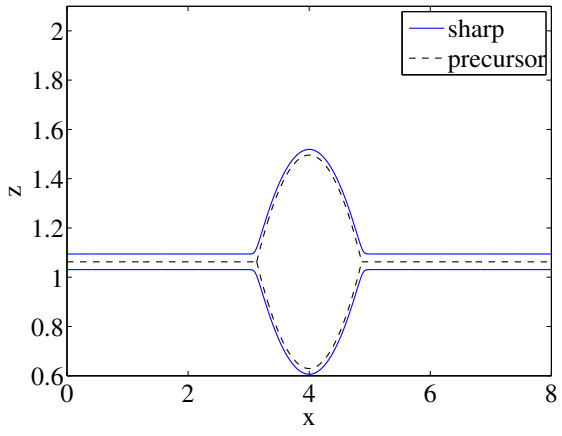


Figure 6: Stationary solutions of sharp triple-junction transient solutions from example 3.1 (solid lines) with $h_1^*(0, x) = h_1 - h_*/2, h^*(0, x) = h + h_*/2$ as initial data for the precursor problem and $h_* = 1/16$ (dashed lines).

We study instationary solutions of example 3.1 in order to provide a comparison of the sharp triple-junction model with those of the precursor model. As initial data for the precursor model we used $h_1^*(0,x) = h_1(0,x) - h_*/2$ and $h^*(0,x) = h(0,x) + h_*/2$ with $h_* = 1/512$ and $h_* = 1/16$. In the implementation of the sharp-interface model we start with time-step sizes $\tau = 10^{-6}$ and perform $n_t = 300$ iteration. Afterwards we successively increase $\tau \to 10\tau$ and repeat that procedure until we are sufficiently close to the stationary states. Corresponding solutions of both models and at different times are shown in figure 7. The left panel shows the solution and the right panel shows a close-up of the triple-junction. For $t \ll 1$ the solutions of both models shown in figure 7 are very close, difference are only visible on the scale $10^{-3}$. At larger times numerical solutions deviate, where the general structure of the solution seems to remain the same but the gradient formulation is ahead in time. For example it reaches the stationary state at $t \sim 10$ and $h_1$ is almost flat in the region $\omega_1 \cup \omega_3$, whereas $h_1^*$ of the precursor model is still curvy. Looking at the excellent agreement at early times where both methods use small time-steps we propose that this difference is due to the implicit time-step overdamping the evolution in the precursor model. To overcome this problem a different time-integration scheme should be used.

As expected, stationary solutions show an excellent agreement and differences are mainly due to mass differences due to the definition of the precursor. In figure 6 a stationary solution with a rather big precursor $\varepsilon = 1/16$ is compared with a stationary solution of the gradient formulation.

## 4.2 Source-type solutions for $\sigma = 0$

In order to validate the gradient model and to show its capabilities we will derive source-type solutions of (2) in this section and compare with numerical solutions. As a class of special solutions featuring contact-line motion source-type solutions on solid substrate have gotten some attention in the past. On a solid substrate it is known that the exponent in the mobility matrix $q(h) = h^\nu$ in the thin-film equation

$$\partial_t h - \nabla \cdot (q \nabla \pi) = 0, \qquad \pi = -\Delta h$$

determines properties of solutions. Bernis et al. [20] proved that for each $0 < \nu < 3$ there is a unique even solutions and it has compact support. For $\nu \geq 3$ they prove nonexistence of nontrivial solutions. The structure of solutions near the triple-junction (solid/liquid/air) was worked out by Giacomelli et al. [21]. In the context of bilayer flows we seek source-type solution $h_1(t,x), h(t,x)$ of the special form

$$h_1(t,x) = 1 - H(\eta) t^{-\alpha}, \qquad h(t,x) = G(\eta) t^{-\alpha}$$

where $\eta = x t^{-\alpha}$ and $\alpha > 0$. The approximation we are going to make assume $t \to \infty$ and thereby $H t^{-\alpha} \ll 1$. Plugging this ansatz into (2) we obtain

$$\alpha t^{-\alpha-1} (\eta H)' = t^{-2\alpha} \left( Q_{11} \pi_1' + Q_{12} \pi_2' \right)', \tag{23}$$

$$-\alpha t^{-\alpha-1} (\eta G)' = t^{-2\alpha} \left( Q_{21} \pi_1' + Q_{22} \pi_2' \right)', \tag{24}$$

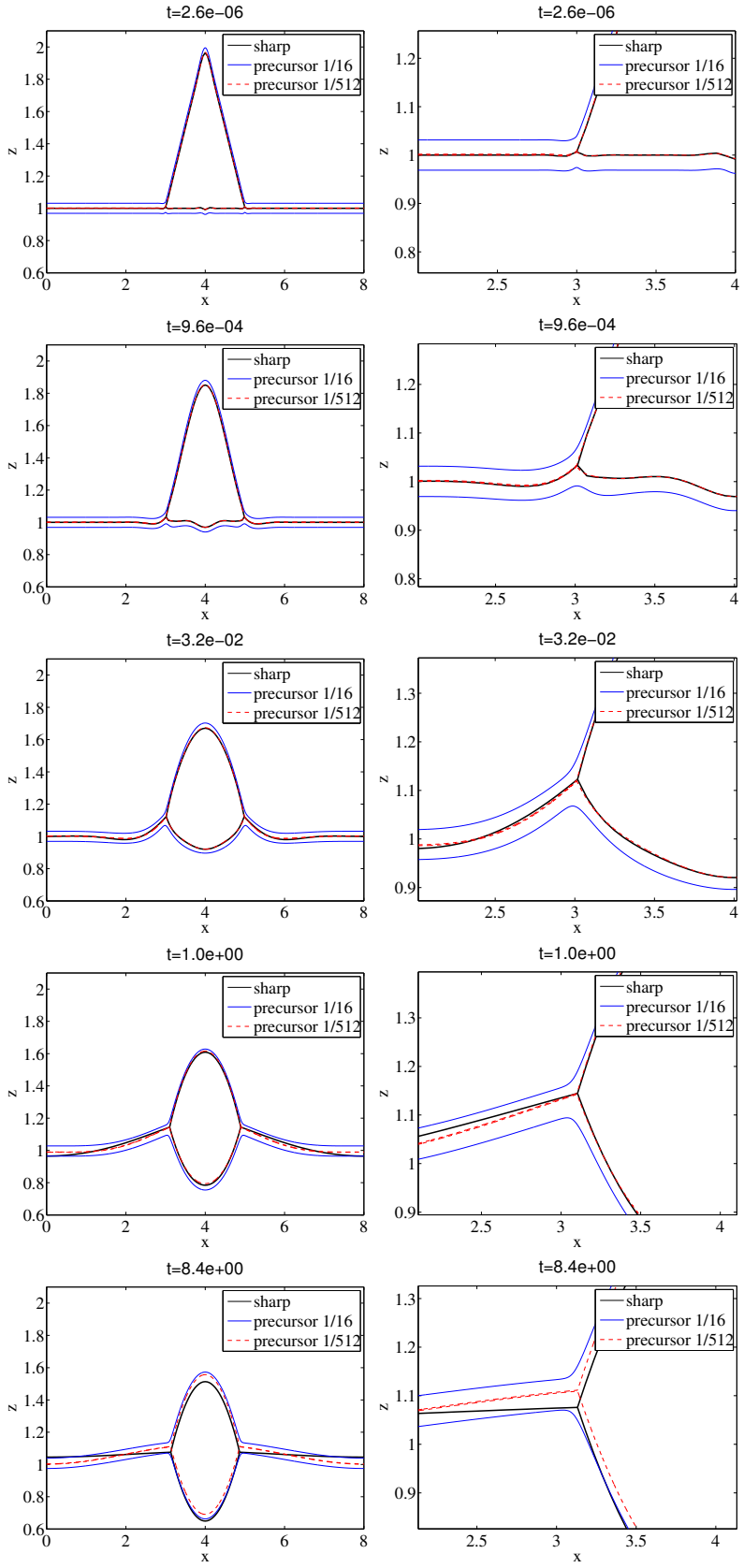


Figure 7: Evolution of gradient model and precursor model at different times. For $t < 10^{-2}$ solutions of both models are nearly indistinguishable.

where $(.)' = \partial_\eta(.)$. The mobility matrix reads

$$Q = \frac{1}{\mu}\begin{pmatrix} \frac{1}{3}(1-H(\eta)t^{-\alpha})^3 & \frac{1}{2}(1-H(\eta)t^{-\alpha})^2 G(\eta)t^{-\alpha} \\ \frac{1}{2}(1-H(\eta)t^{-\alpha})^2 G(\eta)t^{-\alpha} & \frac{\mu}{3}(G(\eta)t^{-\alpha})^3 + (1-H(\eta)t^{-\alpha})(G(\eta)t^{-\alpha})^2 \end{pmatrix}$$

and the generalized pressures are

$$\pi_1 = \big((\sigma_1+\sigma_2)H''' - \sigma_2 G'''\big)t^{-3\alpha}, \quad \pi_2 = \sigma_2\big(H''' - G'''\big)t^{-3\alpha}. \tag{25}$$

Now, we balance our equations such that the leading order of mobility matrix $Q$ does not become singular. To ensure this we let $\alpha$ fulfill $-\alpha - 1 = -7\alpha$, that is $\alpha = 1/6$. Asymptotic expansions of $H$ and $G$ with respect to $t^{-\alpha}$, i.e. $H = H_0 + t^{-\alpha}H_1 + o(t^{-\alpha})$, $G = G_0 + t^{-\alpha}G_1 + o(t^{-\alpha})$, give the leading order equation

$$0 = \big((\sigma_1+\sigma_2)H_0''' - \sigma_2 G_0'''\big)''. \tag{26}$$

Since for large times we expect $h_1$ to become flat on the $\omega_1 \cup \omega_3$ we get

$$H_0 = \frac{\sigma_2}{\sigma_1+\sigma_2}G_0. \tag{27}$$

The function $G_0$ will be derived from the next order

$$0 = \left(\frac{1}{3\mu}\big((\sigma_1+\sigma_2)H_1''' - \sigma_2 G_1'''\big)' + \frac{\sigma_2}{2\mu}G_0\big(H_0''' - G_0'''\big)'\right)', \tag{28}$$

$$-\frac{1}{6}(\eta G_0)' = \left(\frac{1}{2\mu}G_0\big((\sigma_1+\sigma_2)H_1''' - \sigma_2 G_1'''\big)' + \frac{\sigma_2}{\mu}G_0^2\big(H_0''' - G_0'''\big)'\right)'. \tag{29}$$

Putting the last three equations together we get

$$(\eta G_0)' = \left(\frac{3\sigma_1\sigma_2}{2\mu(\sigma_1+\sigma_2)}G_0^2 G_0'''\right)'. \tag{30}$$

This is the equation for source-type solutions with $\alpha = 2$. The difference to thin-films on a solid substrate is that this solution is only asymptotically valid, when $Ht^{-\alpha} \ll 1$. For short times higher order corrections $G_1, G_2, ...$ would be needed to improve the accuracy of solutions. In figure 8 we show half-width of the spreading droplet $(x_+ - x_-)/2$ for a solution with initial data $h = (1-x)_+$ and $h_1 = 1 - h/2$ in $\omega = (-150, 150)$. The time-steps are increased according to the power-law to avoid contact line motion to become too fast or too slow. The solution at different times is shown in figure 9. Note that even though the $t^{1/6}$ power-law of figure 8 sets in already at $t \sim 10^2$, the solutions resemble the source-type solution with $h_1 \equiv 1$ for $x > x_+$ or $x < x_-$ only for $t \gtrapprox 10^8$.

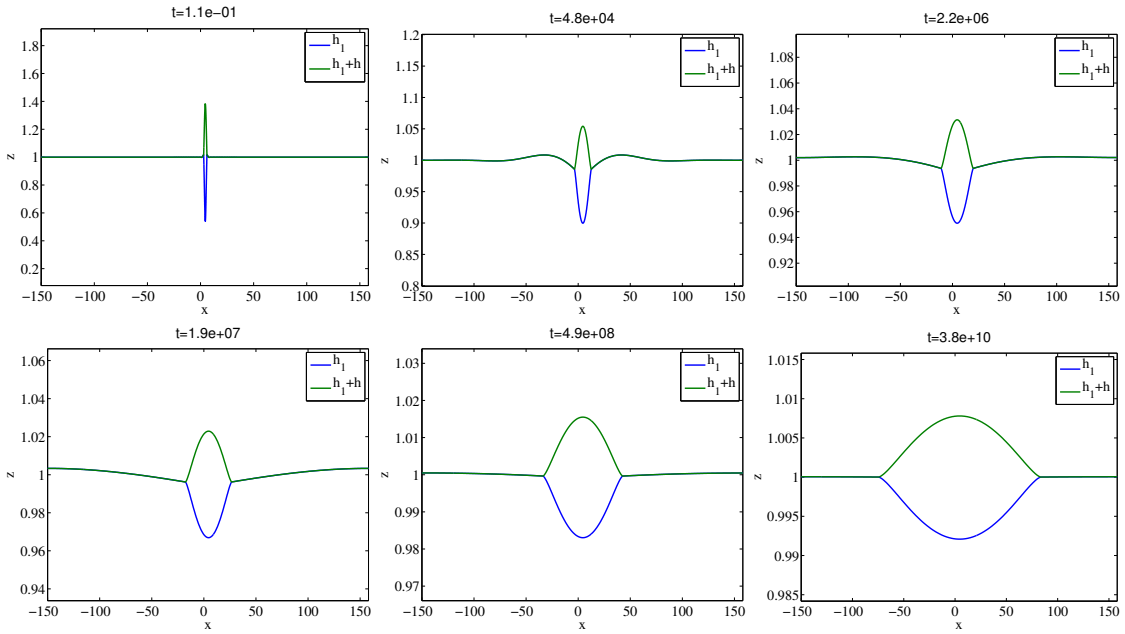


Figure 9: Spreading of droplet converging to a source-type solution. Note that the scales change as $t \to \infty$. The total volume of both liquids is conserved with a relative precision $(m_i(0) - m_i(t))/m_i(0) \sim 10^{-3}$ for $0 < t < 10^{10}$.

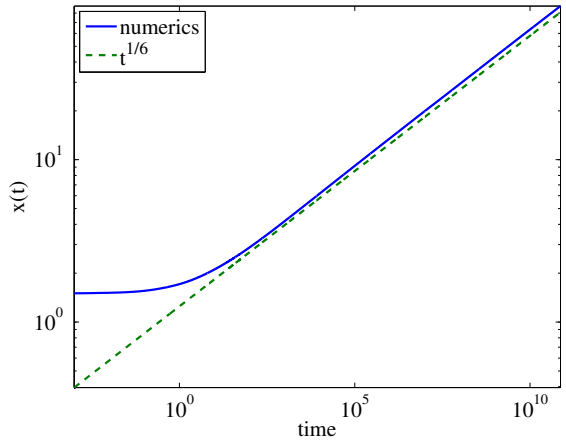


Figure 8: Half-width of the spreading droplet $(x_+ - x_-)/2$ as a function of time shows the predicted $t^{1/6}$ power law.

As one can clearly see that the contact line nicely resembles the expected power-law for sufficiently large times. What is known about the solution $G_0$ is that

$$G_0(\eta) = A(\eta \pm \eta_0)^{3/2}(1 + o(\eta \pm \eta_0)$$

as $\eta \to \pm\eta_0$ where $\eta_0$ is the rescaled position of the triple-junction.

Since the equation is scaling-invariant we can set $\eta_0 = 1$. The function $G_0$ can be easily determined by a boundary value problem which we solve using a Runge-Kutta ODE integrator

of $5$th order combined with a shooting method. The comparison of both rescaled profiles $G_0$ and the rescaled profile from the gradient model are shown in figure 10. The remaining differences are probably due to the fact that with $h \sim 10^{-2}$ the solution still requires higher order corrections and the mesh for solving the PDE was quite coarse. Note that the PDE solution shows the above-mentioned behavior $(\eta \pm \eta_0)^{3/2}$. We are unable to compare higher order corrections $o(\eta \pm \eta_0)$ also because the used mesh was rather coarse, but we showed the capability of the gradient approach to capture the motion of the triple-junction for zero contact angle and also to capture the corresponding singularity $G_0(\eta) \sim (\eta \pm \eta_0)^{3/2}$. This is of course a necessary prerequisite for a sharp-interface gradient model.

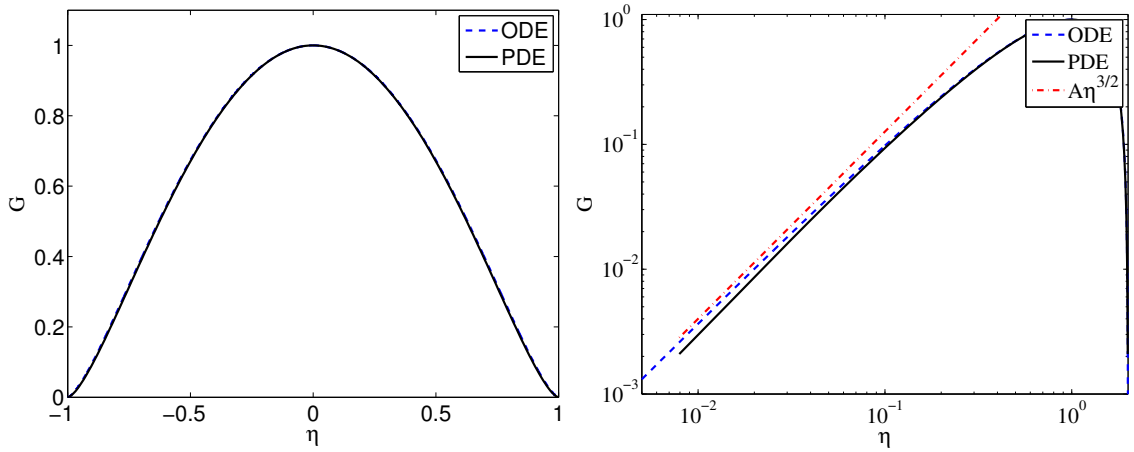


Figure 10: (left) Comparison of PDE solution with ODE solution and (right) comparison near $\eta' = \eta + 1 \sim 0$

# 5 Conclusion

Starting from gradient flow formulation of a two-phase Stokes flow we motivated a corresponding gradient structure for a thin-film bilayer model. In both models the triple-junction is treated explicitly. Boundary conditions at the triple-junction followed either from the definition of the solution manifold or from the gradient of the surface energy. We identified the resulting gradient with the well known model for sharp-interface bilayer flow of Kriegsmann [7].

The gradient formulation admits a natural discretization in a finite element framework, where constraints of the solution space are enforced by Lagrange multipliers on a discrete level. We showed that the algorithm is robust in terms of the solution quality for large time-steps and on coarse grids and can be extended to 3D. We compared numerical solutions of the sharp-interface model with those of the precursor model and found excellent agreement for short and moderate times. However, for large times solutions of the precursor model seemed to be overdamped. Furthermore we confirmed convergence of numerical solutions of the gradient model to asymptotic source-type solutions for quadratic mobility and find excellent agreement in terms of the power-law and the shape of the source-type solution for $t \to \infty$. All this leads us to believe that the sharp-interface gradient formulation is a useful technique to model spreading

and dewetting of bilayer flows and is also a natural structure for numerical algorithms.

## Acknowledgements

SJ and DP thank the German Research Foundation DFG for financial support through the project *Structure formation in thin liquid-liquid films* in the SPP 1506 and DFG Research Center MATHEON through the project C10. The work of GK was supported by the postdoctoral scholarship at the *Max-Planck-Institute for Mathematics in the Sciences* in Leipzig. We also thank Maciek Korzec (Technical University Berlin) for useful discussions.

## References

[1] A. Oron, S.H. Davis, and S.G. Bankoff. Long-scale evolution of thin liquid films. *Reviews of Modern Physics*, 69(3):931, 1997.

[2] C. Huh and L.E. Scriven. Hydrodynamic model of steady movement of a solid/liquid/fluid contact line. *Journal of Colloid and Interface Science*, 35(1):85–101, 1971.

[3] H. Hervet and P.G. de Gennes. The dynamics of wetting: precursor films in the wetting of dry solids. *Comptes Rendus de l'Académie des Sciences*, 299:499–503, 1984.

[4] P.G. de Gennes, F. Brochard-Wyart, and D. Quéré. *Capillarity and wetting phenomena: drops, bubbles, pearls, waves*. Springer, 2004.

[5] J.F. Joanny. Wetting of a liquid substrate. *Physicochemical Hydrodynamics*, 9(1-2):183–196, 1987.

[6] F. Brochard-Wyart, P. Martin, and C. Redon. Liquid/liquid dewetting. *Langmuir*, 9(12):3682–3690, 1993.

[7] J.J. Kriegsmann and M.J. Miksis. Steady motion of a drop along a liquid interface. *SIAM Journal on Applied Mathematics*, pages 18–40, 2003.

[8] A. Pototsky, M. Bestehorn, D. Merkt, and U. Thiele. Alternative pathways of dewetting for a thin liquid two-layer film. *Physical Review E*, 70(2):025201, 2004.

[9] R.V. Craster and O.K. Matar. On the dynamics of liquid lenses. *Journal of Colloid and Interface Science*, 303(2):503–516, 2006.

[10] G. Karapetsas, R.V. Craster, and O.K. Matar. Surfactant-driven dynamics of liquid lenses. *Physics of Fluids*, 23(12):122106–122106, 2011.

[11] K.D. Danov, V.N. Paunov, N. Alleborn, H. Raszillier, and F. Durst. *Stability of evaporating two-layered liquid film in the presence of surfactant*. *Chemical engineering science*, 53(15):2809–2822, 1998.

[12] J.J. Kriegsmann. *Spreading on a liquid film*. PhD thesis, Northwestern University, 1999.

[13] S. Jachalski, G. Kitavtsev, and R. Taranets. Weak solutions to lubrication systems describing the evolution of bilayer thin films. Technical report, 2012.

[14] J. Escher and B.V. Matioc. *Non-negative global weak solutions for a degenerated parabolic system approximating the two-phase Stokes problem*. *arXiv preprint arXiv:1210.6457*, 2012.

[15] D. Merkt, A. Pototsky, M. Bestehorn, and U. Thiele. Long-wave theory of bounded two-layer films with a free liquid–liquid interface: short-and long-time evolution. *Physics of Fluids*, 17:064104, 2005.

[16] F. Otto. The geometry of dissipative evolution equations: the porous medium equation. 2001.

[17] M. Rumpf and O. Vantzos. Numerical gradient flow discretization of viscous thin films on curved geometries. *Mathematical Models and Methods in Applied Sciences*, 23(05):917–947, 2013.

[18] J.W.S. Rayleigh. On the motion of a viscous fluid. *Philosophical Magazine*, 6(26):621–628, 1913.

[19] F.E. Neumann. Vorlesung über die Theorie der Capillarität. *BG Teubner: Leipzig*, pages 113–116, 1894.

[20] F. Bernis, L.A. Peletier, and S.M. Williams. Source type solutions of a fourth order nonlinear degenerate parabolic equation. *Nonlinear Analysis: Theory, Methods & Applications*, 18(3):217–234, 1992.

[21] L. Giacomelli, M. Gnann, and F. Otto. Regularity of source-type solutions to the thin-film equation with zero contact angle and mobility exponent between 3/2 and 3. 2012.